

1 **~~Brief Communication:~~ Evaluating Snow Depth Measurements from**
2 **Ground-Penetrating Radar and Airborne Lidar in Boreal Forest and**
3 **Tundra Environments during the NASA SnowEx 2023 Campaign**

4 Kajsa Holland-Goon¹, Randall Bonnell^{2,1}, Daniel McGrath¹, W. Brad Baxter³, Tate Meehan⁴, Ryan
5 Webb⁵, Christopher F. Larsen⁶, Hans-Peter Marshall⁷, Megan Mason^{8,9}, Carrie Vuyovich⁸

6 ¹Department of Geosciences, Colorado State University, Fort Collins, Colorado, USA

7 ²U.S. Geological Survey, Water Resources Mission Area, Denver, Colorado, USA

8 ³Cold Regions Research and Engineering Laboratory, U.S. Army Corps of Engineers, Fairbanks, Alaska, USA

9 ⁴Cold Regions Research and Engineering Laboratory, U.S. Army Corps of Engineers, Hanover, New Hampshire, USA

10 ⁵Department of Civil and Architectural Engineering & Construction Management, University of Wyoming, Laramie,
11 Wyoming, USA

12 ⁶Geophysical Institute, University of Alaska, Fairbanks, Alaska, USA

13 ⁷Department of Geosciences, Boise State University, Boise, Idaho, USA

14 ⁸Hydrological Sciences Laboratory, NASA Goddard Space Flight Center, Greenbelt, Maryland, USA

15 ⁹Science Systems Applications Inc., Lanham, Maryland, USA

16 *Correspondence to:* ~~Kajsa Holland-Goon~~Randall Bonnell (~~khollgoon@gmail.com~~rbonnell@usgs.gov), Daniel McGrath
17 (daniel.mcgrath@colostate.edu)

19 **Abstract.** We evaluated ground-penetrating radar (GPR) and airborne lidar retrievals of snow depth collected during the
20 NASA SnowEx 2023 campaign in ~~Alaskan~~ tundra and boreal forest environments in Alaska along 44 short (3–12 m) transects.
21 Compared to in situ observations, we identified modest biases for GPR snow depths (bias <0.03 m in tundra, +0.06 m in boreal
22 forests) and larger biases for lidar snow depths in the boreal forests (bias +0.19 m at a tundra site, ~~(-0.16 m in boreal forests)~~.
23 At the Upper Kuparuk-Toolik tundra site, lidar snow depths exhibited a small bias (-0.02 m), whereas the bias was much
24 larger at the Arctic Coastal Plain tundra site (+0.19 m). For most sites, biases were primarily related to sub-snow vegetation,
25 tussocks, and seasonally dynamic ground. However, we identified vertical alignment issues with the Arctic Coastal Plain lidar
26 snow depth dataset that likely contributed to the higher bias. These complex ground surface and sub-snow vegetation in these
27 environments present a challenge to established snow depth measurement methods, which needs to be considered when
28 evaluating novel remote sensing approaches.

29 **1 Introduction**

30 In high-latitude (>60°) terrestrial systems, snow plays a crucial role in the hydrologic cycle and modulates the surface energy
31 balance. Snow ~~also~~ strongly impacts the ecology of these regions: snow influences caribou winter range selection (Duquette,
32 1988; Pedersen et al., 2021) and vegetation phenology (Kelsey et al., 2021), and provides winter refuges for a diverse range
33 of animals (Aitchison, 1987; Penczykowski et al., 2017). Snow cover extent in the Arctic has experienced dramatic reductions
34 during the satellite era, with observed declines of -3.5% and -13.4% per decade in May and June, respectively (Meredith et
35 al., 2019). Given the vast spatial scales and sparse in situ station network, remote sensing can play a critical role in snowpack
36 monitoring in these sensitive environments.

37 The NASA SnowEx 2023 campaign was implemented to improve the understanding of remote sensing methods for
38 retrievals of snow depth and snow water equivalent (SWE), the mass of the snowpack, in tundra and boreal forest environments
39 (Vuyovich et al., 2024). These regions are understudied relative to temperate mountains; for instance, they are currently not
40 included in gridded SWE analysis products (e.g., SNODAS). ~~Space-borne~~ remote sensing retrievals of snow depth or SWE at
41 high spatial resolution may be achievable in these complex environments through lidar or radar methods (Fair et al., 2025;
42 Eppler et al., 2022), but further evaluation of the uncertainties caused by the unique physical parameters within these
43 environments (e.g., dense canopy cover and ground vegetation) is required.

44 The boreal forest is characterized by a dense canopy of coniferous and deciduous trees and covers 10–17% of the world’s
45 landmass (NASA Earth Observatory, 2006; Vuyovich et al., 2024). Boreal forest seasonal snowpacks are typically shallow
46 (<1.2 m) and exhibit lower snow densities due to minimal wind loading, cold temperatures, and large temperature gradients in
47 the snowpack, resulting in extensive faceting (Pruitt, 1970 ~~Sturm and Liston, 2021~~). In contrast, the Arctic tundra extends to
48 higher latitudes than boreal forests and is subject to extreme cold temperatures and high winds that limit plant growth. Tundra
49 snowpacks are typically shallower than boreal forest snowpacks, but wind redistribution can build deep snow drifts (Benson,
50 1967; Benson and Sturm, 1993 ~~Sturm and Liston, 2021~~). Because of wind-driven compaction, tundra snowpacks can exhibit

51 higher densities than snowpacks in the boreal forest and include a binary stratigraphy of high-density wind slab above low-
52 density, large-grained depth hoar. Both environments have features that may complicate snow depth retrievals from lidar or
53 radar methods. In boreal forests, ~~dense~~thick forest canopy, canopy-intercepted snow, and dense shrub and tussock (i.e., small
54 localized tufts of grass or sedge~~areas~~ where the solid ground is raised) cover may occlude lidar, whereas dense shrub cover
55 can cause a void space between the bottom of the snowpack and the ground, leading to a mismatch between the more easily
56 identified radar ground reflector and the true base of the snowpack. Tundra environments contain spatially varying distributions
57 of shrub and tussock cover that may increase uncertainty of lidar or radar methods. Additionally, the North Slope tundra
58 ~~environments~~ground surface is complex and experiences seasonal fluctuations driven by freeze-thaw processes. These
59 environments contain hummocks, ice wedges, ice polygons, and are underlain by shallow permafrost (Jorgenson et al., 2008)
60 ~~and exhibit seasonal thaw cycles (e.g., thaw subsidence)~~. This dynamic ground surface can ~~increase~~cause increased lidar snow
61 depth uncertainty because of differences in the ground elevation between snow-on and snow-off lidar acquisitions (Chen et
62 al., 2020). In both environments, frozen soil may have similar dielectric properties to the snowpack, and thus can cause variable
63 the radar signal can~~penetration~~penetrate below the snow-ground interface.

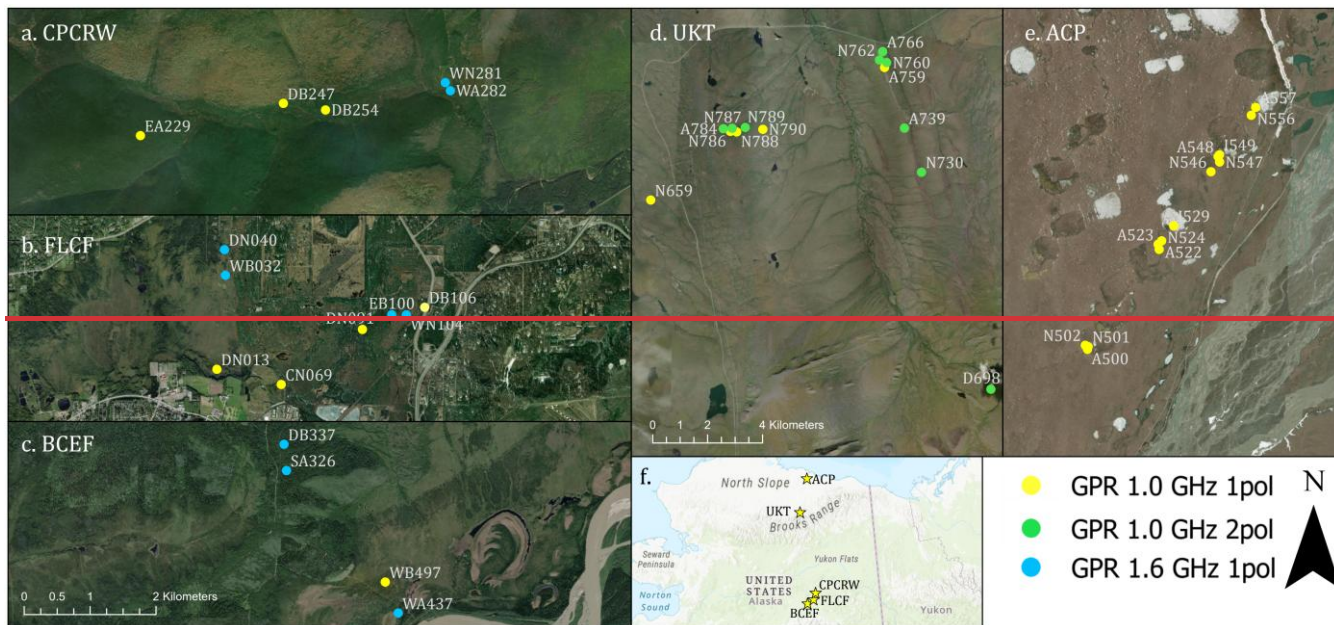
64 During NASA SnowEx 2023 in Alaska, we conducted detailed in situ surveys to improve our understanding of radar and
65 lidar performance for snow depth retrieval in these complex high-latitude environments. Here, we evaluate ground-based radar
66 and airborne lidar snow depth products along transects where manual measurements of snow depth were collected after snow
67 excavation. The excavated snow depths represent the integrated thickness of the snowpack, which excludes intra- and sub-
68 snowpack void spaces. In particular, we emphasize how sub-snow vegetation and variable ground conditions associated with
69 mosses, tussocks, and/or permafrost influence the retrieval accuracy.

70

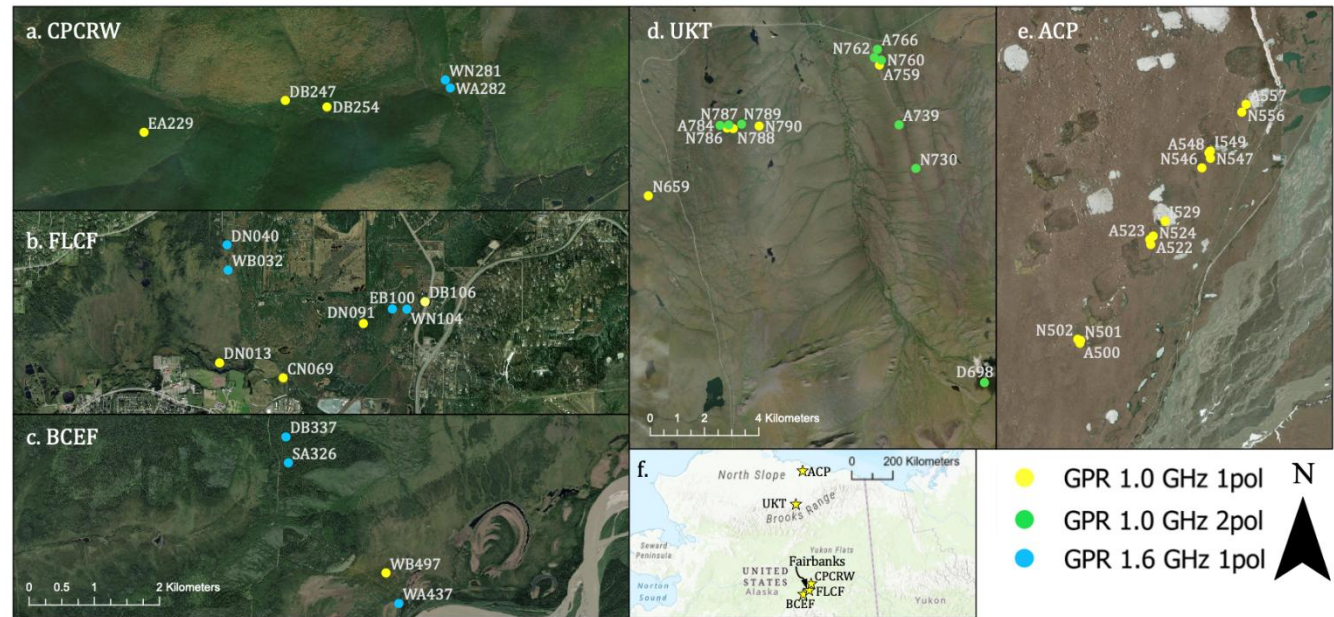
71 **2 Study Sites**

72 The NASA SnowEx 2023 Alaska campaign (7–16 March 2023) was operated at three field sites in the boreal forests near
73 Fairbanks (Figure 1a–c) and two sites in the Arctic tundra on the North Slope (Figure 1d, e). Although some snowmelt was
74 observed in the boreal forest canopy, the snowpack on the ground was considered dry based on snow pit temperature
75 measurements. Of the boreal forest sites, the Caribou/Poker Creek Research Watershed site (CPCRW; Figure 1a) is located
76 ~25 km northeast of Fairbanks and hosted eight surveys, the Farmers Loop Experimental Station and Creamer’s Field
77 Migratory Waterfowl Refuge (FLCF; Figure 1b) north of Fairbanks hosted six surveys, and the Bonanza Creek Experimental
78 Forest (BCEF; Figure 1c) is ~20 km southwest of Fairbanks and hosted four surveys. Vegetation varied by site: CPCRW
79 surveys were performed primarily below black spruce canopy, FLCF included transects within black spruce (*Picea mariana*),
80 deciduous, mixed canopy, and agricultural field environments, and BCEF surveys were performed primarily below leaf-off
81 deciduous canopy and in wetland shrub environments (Vuyovich et al., 2024). Surveys at the Upper Kuparuk-Toolik site
82 (UKT; Figure 1d) had ground conditions that varied from shrubs and tussocks to frozen ponds, whereas the Arctic Coastal

83 Plain site (ACP; Figure 1e), located near Deadhorse, primarily included surveys performed in wetlands and frozen ponds/lakes
 84 (Vuyovich et al., 2024). The sites near Fairbanks are within the discontinuous permafrost region (Jorgenson et al., 2008),
 85 whereas both UKT and ACP are underlain by continuous permafrost (Obu et al., 2019).
 86



87



88

89

90 **Figure 1: Ground surveys at the (a) Caribou/Poker Creek Research Watershed (CPCRW), (b) Farmers Loop/Creamer’s Field**
91 **(FLCF), (c) Bonanza Creek Experimental Forest (BCEF), (d) Upper Kuparuk-Toolik (UKT), and (e) Arctic Coastal Plain (ACP)**
92 **field sites. (f) Map inset depicts the locations of the five field sites within Alaska. Imagery provided by ESRI, Maxar and Microsoft.**

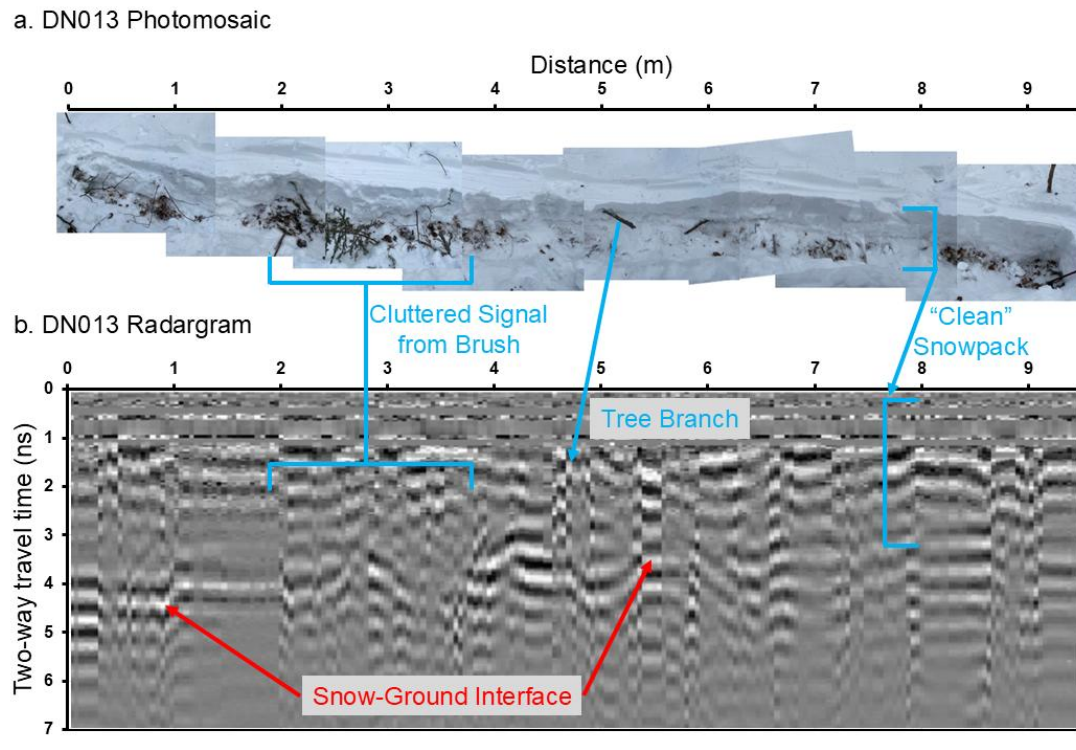
93 **3 Methods**

94 **3.1 Summary of Field and Airborne Lidar Surveys**

95 We operated four ground-penetrating radar (GPR) systems to cover the five field sites, including two surface-coupled 1.0 GHz
96 center-frequency PulseEkko Pro single transceiver/receiver systems, an air-coupled 1.0 GHz center-frequency PulseEkko Pro
97 single transceiver with dual polarization receivers system, and a surface-coupled 1.6 GHz GSSI single transceiver/receiver
98 system. The PulseEkko Pro systems have a 6 dB bandwidth of 500–1500 MHz, whereas the GSSI system has a 6 dB bandwidth
99 of 800–2400 MHz. Each GPR used a GNSS system to provide locations for collected traces: the air-coupled PulseEkko Pro
100 used a Geode dGPS system (± 0.5 m accuracy), the two sled-coupled PulseEkko Pro GPRs used Emlid RS2 rovers with Emlid
101 RS2 bases located nearby for post-kinematic processing (± 0.5 m accuracy), and the sled-coupled GSSI GPR used a mapping-
102 grade GPS system (± 3 m accuracy). In Figure 1, each transect is marked by the associated GPR system.

103 ~~We operated four different GPR systems across the various field sites. Details are provided in Text S1.~~ For the three
104 surface-coupled GPR surveys, the GPR was pulled across the surface of the snowpack in a sled, whereas the air-coupled GPR
105 was carried by two people above the snow surface. GPR systems were operated in the common-offset configuration and we
106 took care not to disturb the snowpack immediately below the GPR transect. Transect lengths ranged from 3–12 m.
107 Methods for deriving GPR snow depths are provided in Text S1-Section 3.2. Following GPR data collection, the snow along
108 the full length of the transect was excavated and snowpack thicknesses, which excluded any void spaces or tree branches
109 or logs in the snowpack, were measured at 0.25–1 m intervals. A recent study supports this methodology because void spaces
110 can be identified and subtracted from the measured depths (Stuefer et al., 2025). Pictures and/or video recordings were acquired
111 for each transect and detailed notes were taken on vegetation and ground conditions. An example photomosaic of an excavated
112 boreal forest transect is provided in Fig. S12. Each survey was completed within 15 m of a snow pit, wherein measurements
113 of snow depth, snow density, SWE, and snow temperatures were collected. In total, 17 surveys were collected at the boreal
114 forest field sites and 27 surveys were collected at the tundra field sites on the North Slope. At each field site, snow-on airborne
115 lidar surveys were collected during the campaign and snow-off airborne lidar surveys were collected during the following
116 summer. Snow-on and snow-off lidar surveys were used to generate 0.5 m snow depth and canopy height models (Larsen,
117 2024). We note that lidar-derived snow depths based on acquisitions that occurred before or after ground surveys have
118 increased uncertainty due to either a changed snow surface (i.e., accumulation, compaction, redistribution) between the lidar
119 flights and ground surveys or snow disturbance caused by the ground observations that preceded lidar flights (n = 20/44).
120 Further processing details for the lidar snow depths are provided in Larsen (2024). A list of lidar and ground survey dates is
121 provided in Table 1 and snow accumulation measurements for every day of the campaign are provided in Table S1.

122



123
124
125
126 **Figure 2: (a) Photomosaic and corresponding (b) radargram of the 9.5 m long Transect-DN013 transect from 7 March 2023 in**
127 **Farmers Loop/Creamer's Field. Annotations illustrate the complexities of GPR collection in the dense brush of boreal forests. In**
128 **particular, we show the signal clutter caused by intra-snowpack vegetation, signal ringing that results from tree branches or tree**
129 **trunks, snow stratigraphy in areas without vegetation ("clean" snowpack), and the location of the snow-ground interface, which**
130 **ranges from ~4 ns near 0 m distance to ~3 ns near 9 m distance.**

131
132
133 **Table 1: Summary of field and airborne survey dates.**

	Field Site	Snow-On Lidar Flight Dates	Ground Survey Dates	Transects (n)
Tundra	Arctic Coastal Plain	10 March 2023	11–14 March 2023	13
	Upper Kuparuk-Toolik	13 March 2023	8–11, 15 March 2023	14

Boreal Forest	Farmers Loop/ Creamers Field	11 March 2023	7–11, 13 March 2023	8
	Bonanza Creek Experimental Forest	11 March 2023	10, 13–15 March 2023	4
	Caribou/Poker Creek Research Watershed	11 March 2023	8–9, 11, 14 March 2023	5

134

135 **3.2 Sources of Ground-Penetrating Radar Processing and Sources of Snow Depth Uncertainty**

136 For GPR systems, the transceiver emits a signal that transmits through the snowpack and reflects off boundaries of contrasting
137 dielectric permittivities (e.g., vegetation, snow stratigraphy, the snow-ground interface). The receiver then records the
138 amplitude and two-way travel times (*twtt*) of these reflections. Radargrams were processed ~~to a trace spacing of and the *twtt*~~
139 ~~of the presumed snow-ground interface were exported at ~0.10 m-spacing, typically identified as the first reflection at depth~~
140 ~~with the highest amplitude that is spatially coherent (further details provided in Text S1). We provide an Examples example~~
141 of ~~two a~~ boreal forest radargrams ~~are provided~~ in Fig. S22.

142 ~~Exported *twtt* of the snow-ground interface, typically identified as the first reflection at depth with the highest amplitude~~
143 ~~that is spatially coherent, were manually selected for all single-polarization GPR datasets (e.g., McGrath et al., 2019). For the~~
144 ~~dual-polarization GPR dataset, *twtt* was obtained by utilizing the coherent reflection between the two receivers (further details~~
145 ~~provided in Meehan et al., 2024). The *twtt* can be converted to snow depth with an estimate of the snowpack radar velocity~~
146 ~~(v_s ; Daniels, 2004)~~

$$147 \quad v_s = \frac{c}{\sqrt{\epsilon_s}}, \quad (1)$$

148 ~~where c is the speed of electromagnetic energy in a vacuum and ϵ_s is the dielectric permittivity of the snowpack. Snowpack~~
149 ~~conditions were dry during our surveys, thus, the relative permittivity can be approximated from the bulk snow density (ρ_s)~~
150 ~~through an empirical relation (Kovacs et al., 1995)~~

$$151 \quad \sqrt{\epsilon_s} = 1 + \frac{0.845 \times \rho_s}{1000}. \quad (2)$$

152 ~~Snow density was sampled in snow pits adjacent to the surveyed transects using 1000 cm³ wedge samplers at 10 cm intervals~~
153 ~~along two columns in the snow pit. If density measurements differed by more than 10% for a single layer, a third measurement~~
154 ~~was acquired. For layers with three measurements, we excluded the measurement with the largest difference. We then~~
155 ~~calculated bulk snow densities as the column average. Finally, snow depth (D_s) is calculated as~~

$$156 \quad D_s = \frac{twtt}{2} \times v_s. \quad (3)$$

157

158 GPR surveys have several sources of uncertainty. GNSS positioning was estimated as ± 0.5 –3 m horizontal accuracy at
159 the boreal forest sites and ± 0.5 m at the Arctic tundra sites, which could complicate the comparison between GPR and lidar
160 snow depths. GPR-derived snow depths may be reduced by up to 0.07 m due to removal and/or compaction of snow as the
161 sled travels across the surface. Finally, site-specific ground conditions may add uncertainty to the GPR snow depths. A few
162 examples include: (1) snow depths may be overestimated because of the presence of void spaces within the snowpack caused
163 by vegetation, (2) snow depths may be underestimated when a dense layer of vegetation obscures the true bottom of the
164 snowpack (e.g., a buried bent-over tree), and (3) snow depths may be overestimated if the radar signal penetrates into frozen
165 soil without a strong reflection at the snow-ground interface.

166 3.3 Evaluation of GPR and Lidar Snow Depths

167 We extracted the lidar snow depths (0.5 m x 0.5 m resolution) along each surveyed transect based on the GNSS coordinates
168 recorded by the GPR. We aligned the excavated depth locations with the GPR depth locations based on field
169 ~~notes measurements~~, resulting in a high-quality co-registration between the GPR and the excavated depths. However, the co-
170 registration between the lidar data and the transect surveys are subject to the GNSSPS uncertainty listed above for the excavated
171 depths that was identical to the GPR. GPR, lidar, and excavated depths were then compared as individual profiles to evaluate
172 any systematic differences. We calculated the mean and standard deviation of snow depth for the GPR, lidar, and in-situ
173 measurements from each transect to estimate the overall root mean squared error (RMSE), bias, and Pearson's correlation
174 coefficient (r) between measurement techniques in both the tundra and boreal forest sites Although both GPR and lidar snow
175 depths likely contain errors and biases, we primarily emphasize bias in the results and discussion because the two are difficult
176 to untangle due to the complex conditions in which these data were collected. Finally, lidar-derived vegetation heights were
177 extracted along each transect in the boreal forest to determine whether accuracy was related to lidar-derived vegetation height.

178 4 Results

179 4.1 Boreal Forest Transects

180 At boreal forest sites, GPR mean snow depths overestimated excavated mean snow depths for 12 of 17 transects, whereas lidar
181 mean snow depths underestimated excavated mean snow depths for 14 of 17 transects (Table S2, Figure 3S3). Large
182 differences (>0.20 m) between GPR and excavated depths occurred where sub-snow shrubs or tree branches caused void spaces
183 in the snowpack (e.g., Figure 3S3g, i), but close agreement was observed for the transect in the agricultural field where only
184 crop stubble was present below the snowpack (Figure 3S3b) and for transects below black spruce canopy (e.g., Figure 3S3n–p).
185 The average residual between GPR and excavated depths was +0.06 m (9% of mean excavated depth) and the average residual
186 between lidar and excavated depths was -0.12 m (16% of overall mean excavated depth) when field surveys occurred after
187 lidar acquisitions (Table S2). For these surveys, the lidar profile either mostly mimicked the excavated depths and agreed
188 within ± 0.07 m (e.g., Figure 3j, 3p), or the lidar profile failed to capture both the spatial patterns and exhibited reduced accuracy

when compared to the excavated depths (e.g., Figure 3h, 3l). The lidar snow depth bias worsened to -0.16 m (24% of mean excavated depth; Table S2) when surveys performed before the lidar survey date were included in the comparison. We visually inspected the boreal forest lidar snow depth rasters to verify the presence of all transects excavated before the 11 March lidar survey and we found that excavation activities clearly influenced five of these surveys. These transects are shown in Fig. S3b, 3d, 3e, 3f, and 3n, illustrating how sample timing can severely bias direct comparisons between field and remote sensing-based depth estimates.

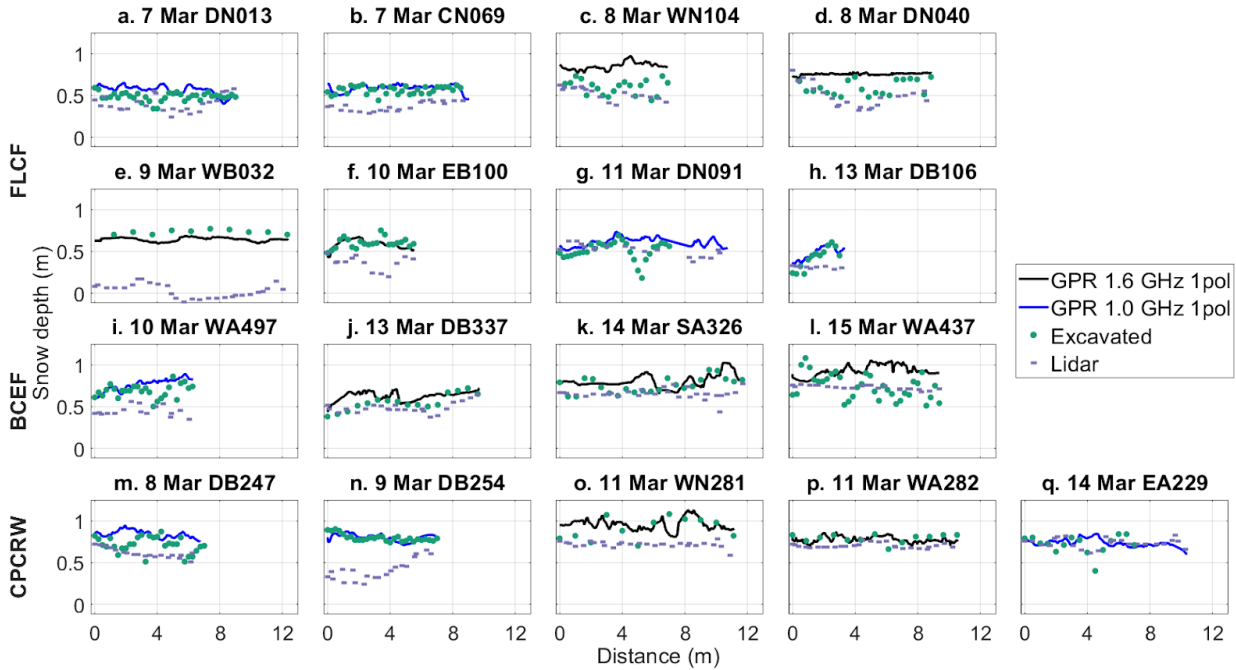
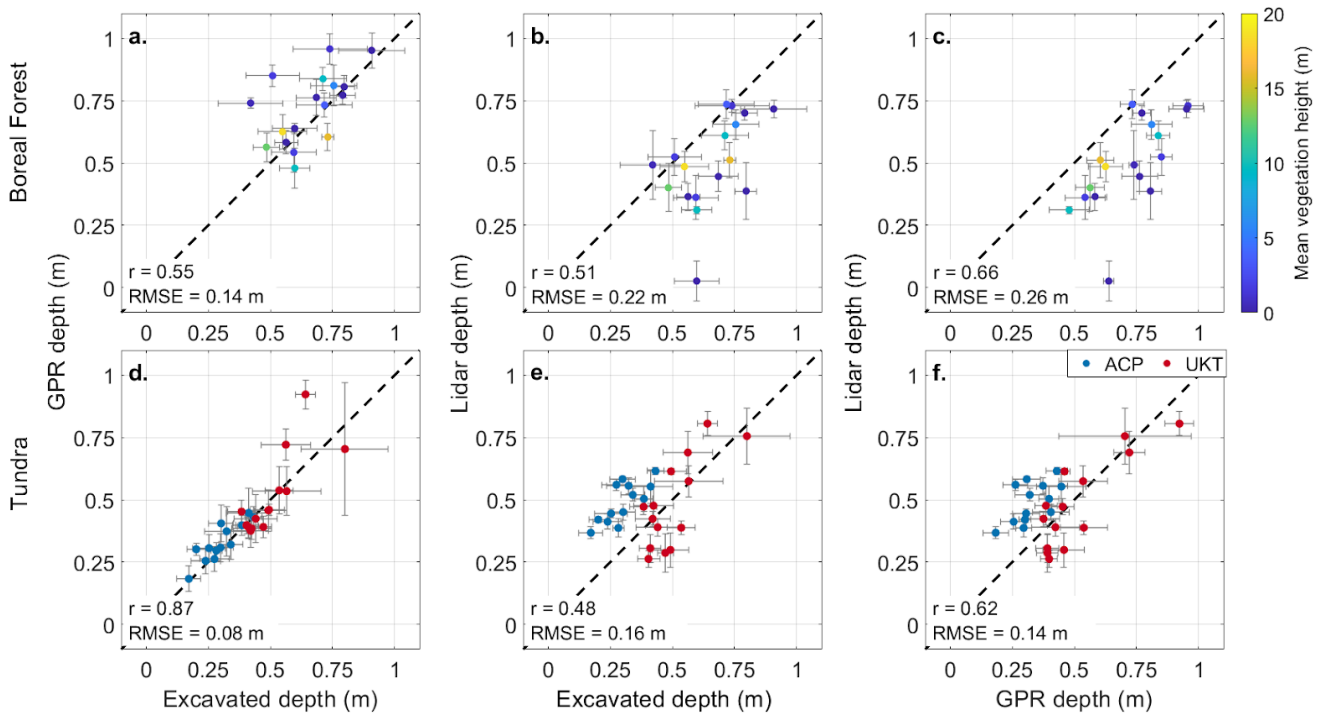


Figure 3: Snow depth profiles at the boreal forest for the (a–h) Farmer’s Loop/Creamer’s Field (FLCF), (i–l) Bonanza Creek Experimental Forest (BCEF), and (m–q) Caribou/Poker Creek Research Watershed (CPCRW) field sites. GPR snow depth profiles were collected by the **CRREL-1.6 GHz GPR system and the **Colorado State University**-1.0 GHz GPR system. Subplots are labeled by transect numbers. Airborne lidar surveys were conducted at all three sites on 11 March 2023.**

Of the three boreal forest field sites, CPCRW yielded the lowest mean GPR residual ($+0.03$ m), whereas BCEF yielded the highest mean residual ($+0.11$ m). Three of the five CPCRW transects were performed below black spruce canopy, where mosses are the dominant substrate and shrub canopy is sparse, whereas shrubs and tussocks dominate the ground below BCEF transects. FLCF surveys (mean GPR residual = $+0.06$ m) were performed primarily below mixed deciduous/coniferous canopy and contained various shrubs, saplings, and tree branches within the snowpack. Compared to GPR, mean lidar residuals exhibited the opposite canopy-driven trend; BCEF surveys yielded the lowest mean residuals (-0.10 m) and FLCF/CPCRW yielded the highest mean residuals (-0.19 m and -0.15 m). However, we note that three of four BCEF surveys were performed after lidar collection, whereas eight of 13 surveys at FLCF/CPCRW were performed before lidar collection (Table S2). Overall,

209 we calculated an r of 0.55 and RMSE of 0.14 m for GPR snow depths and an r of 0.51 and RMSE of 0.22 m for lidar snow
 210 depths at the boreal forest field sites (Figure 42a–b). The best Pearson’s correlation coefficient, but highest RMSE was
 211 observed for the lidar vs. GPR comparison ($r = 0.66$, RMSE = 0.26 m; Figure 42c).
 212



213
 214 **Figure 42:** Comparisons at the boreal forest (a–c) and tundra sites (d–f) between (a, d) GPR and excavated depths, (b, e) lidar and
 215 excavated depths, and (c, f) lidar and GPR depths. The mean values are plotted with error bars calculated from the standard
 216 deviation. Points in a–c are colored by mean lidar-derived vegetation height, which represents the canopy height in forest cover or
 217 the shrub/grass height in meadows. Points in d–f are colored by field site. Sites: ACP, Arctic Coastal Plain; UKT, Upper Kuparuk-
 218 Toolik.
 219

220 4.2 Tundra Transects

221 Vegetation structure was less complex at the Arctic tundra sites than at the boreal forest sites. At ACP, surveys had grassy
 222 ground cover (11 surveys with grass heights of 0.05–0.20 m) or ground ice (two surveys; Figure 5S4i, m), whereas tussocks
 223 (four surveys with tussock heights of 0.08–0.25 m) and shrubs (four surveys with shrub heights <0.30 m) were the predominant
 224 ground cover at UKT. Based on the excavated depths, both mean GPR residuals (ACP = +0.03 ± 0.04 m; UKT = +0.01 ± 0.10
 225 m; Tables S3–S4, Figures S4–S5–6) and the overall performance metrics ($r = 0.87$; RMSE = 0.08; Figure 42d) improved at
 226 the Arctic tundra sites relative to the boreal forest sites.

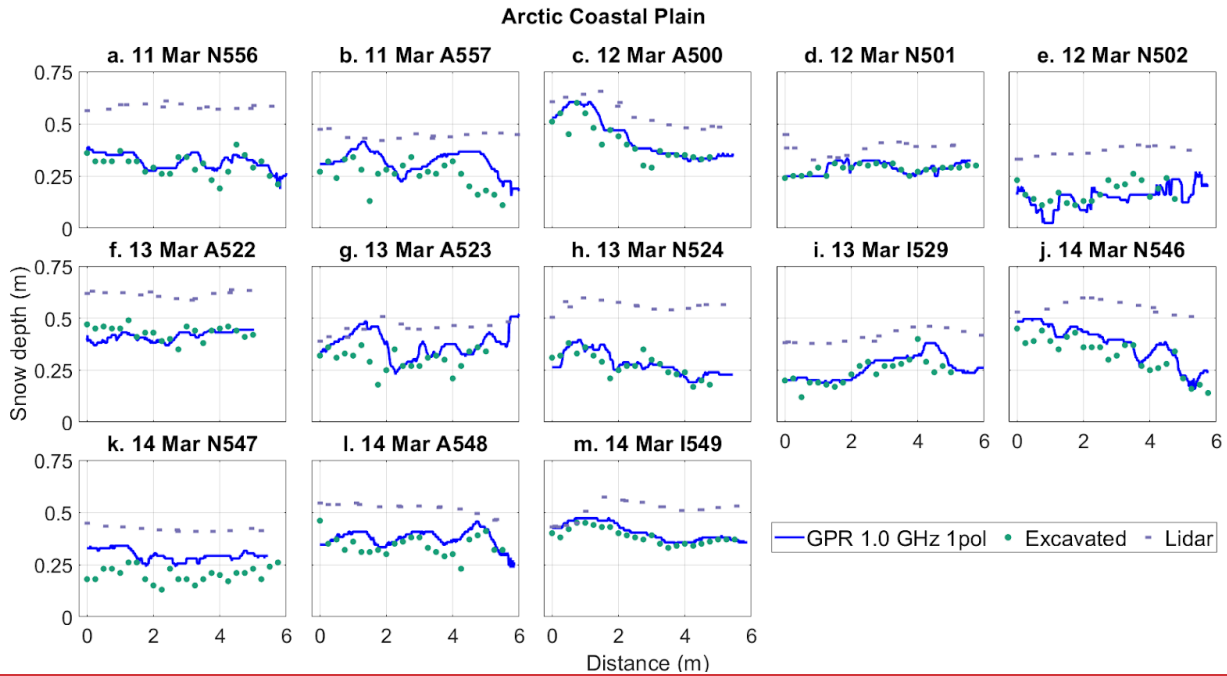
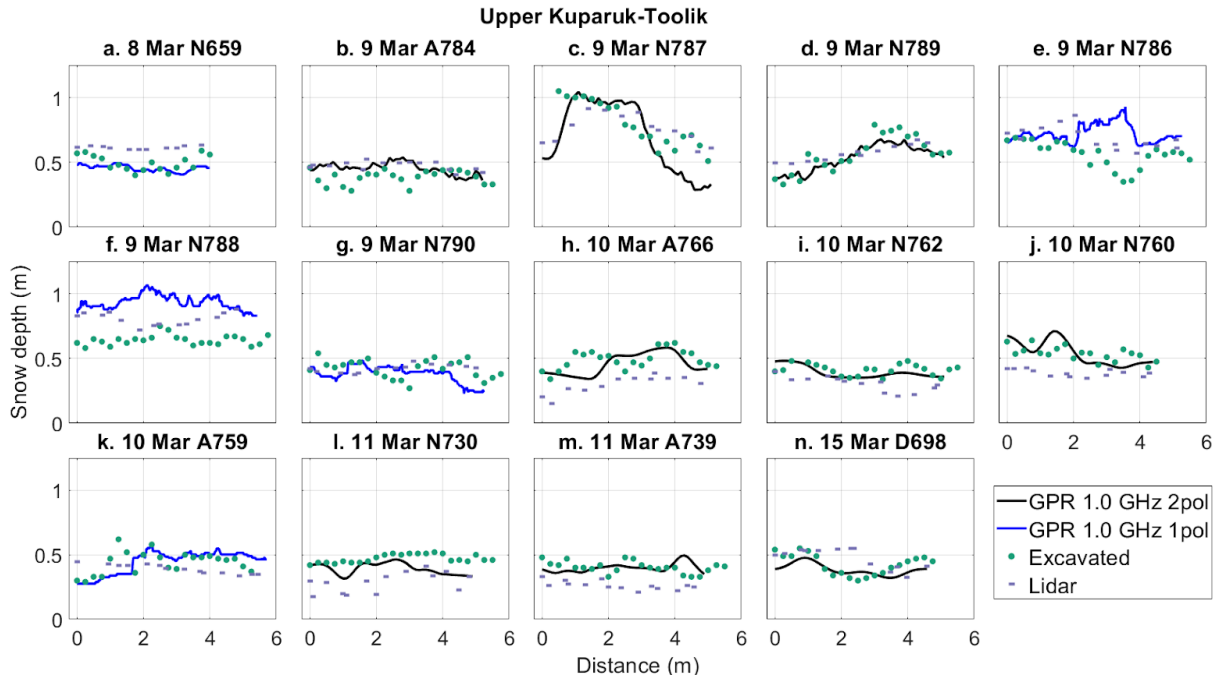


Figure 5: Snow depth profiles at the Arctic Coastal Plain tundra field site organized by date and transect number. GPR snow depth profiles were collected by the single-polarization 1.0 GHz GPR system. Airborne lidar survey was conducted on 10 March 2023.



232 Figure 6: Snow depth profiles at the Upper Kuparuk-Toolik tundra field site organized by date and transect ID. GPR snow depth
233 profiles were collected by the single-polarization 1.0 GHz GPR system and the dual-polarization 1.0 GHz GPR system. Airborne
234 lidar survey was conducted on 13 March 2023.
235

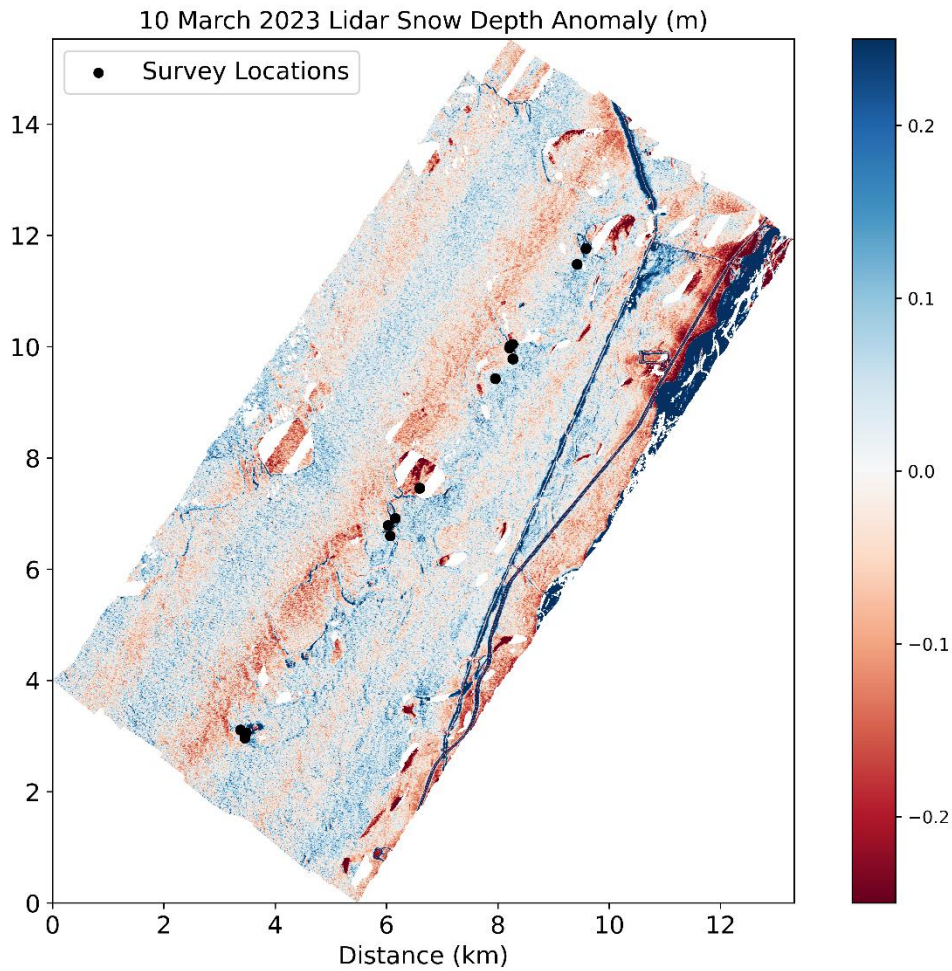
236 Compared to the boreal forest sites, the lidar snow depths from the Arctic tundra sites yielded a comparable Pearson's
237 correlation coefficient, but an improved RMSE ($r = 0.48$; $RMSE = 0.16$ m; Figure 42e). Despite having more complex ground
238 conditions than ACP, UKT yielded the lowest mean lidar residual (ACP = $+0.19 \pm 0.05$ m; UKT = -0.02 ± 0.12 m; Tables S3–
239 S4, Figures S4–S55–6). All ACP lidar profiles exhibited poor magnitude agreement with the excavated depths. Despite this,
240 several of these profiles exhibited spatial patterns that were similar to the excavated depth profiles (Figures 5c, 5f, 5i, 5m)
241 Notably, all ACP surveys were performed after the lidar flight, whereas 13 of 14 UKT surveys preceded the lidar flight (Table
242 1). We visually inspected the transects in the UKT lidar snow depth raster and observed that only five transects were influenced
243 by snow excavation (Figures 6S5h–j, 6l–m).

244 5 Discussion

245 5.1 GPR and Lidar Snow Depth Uncertainty in Boreal Forest and Arctic Tundra Environments

246 We found that GPR captured snow depth variability in both boreal forest and Arctic tundra environments over length scales
247 >0.5 m, but we observed larger uncertainty over shorter length scales (<0.5 m), likely due to the large sensor footprint (~ 1.5
248 m radius for a snow depth of 0.6 m; e.g., Daniels, 2004). GPR snow depths exhibited a modest positive bias ($+0.06$ m) relative
249 to excavated depths in the boreal forest and a smaller positive bias in the Arctic tundra (overall mean residuals = $+1$ – 3 cm;
250 Tables S2, S3). While it is possible that a portion of the observed GPR bias could be explained by differences between the
251 GPR and excavated depth measurement footprints, we largely attribute the positive biases to discontinuous vegetation-
252 induced void spaces at the base and within the snowpack (e.g., Figures S1, S22; Berezovskaya and Kane, 2007). Vegetation
253 was dense and complex in the boreal forest, resulting in cluttered radargrams that were difficult to interpret, whereas Arctic
254 tundra sites had less complex vegetation and better-defined ground reflectors.

255 Lidar at ACP was expected to have the highest agreement with excavated depths because the lidar surveys were conducted
256 before the snowpack was disturbed. Instead, ACP lidar exhibited a $+0.19$ m average bias and failed to reproduce fine-scale
257 snow depth patterns (e.g., Figure 5S4a–b), despite having relatively simpler ground conditions at the time of the surveys. We
258 attribute this to a strip alignment issue in the ACP bare earth elevation model collected in August 2022, which results in linear
259 striping in the snow depths aligned with the lidar swaths. All ground surveys happened to be conducted within a single swath
260 that exhibited higher snow depths (Figure 7), which provides the likely explanation for the observed ACP bias in the snow
261 depths.
262



263
264
265
266 **Figure 7: Lidar snow depth anomalies at ACP with snow depth anomaly saturated between -0.25 and +0.25 m to illustrate the**
267 **linear lidar artifacts oriented southwest to northeast. All GPR transect locations are located within a single swath of the scene.**

268 Although UKT lidar exhibited lower mean bias, it also did not reproduce fine-scale snow depth patterns (e.g., Figure
269 ~~6SSc-f~~). Both ~~sites ACP and UKT~~ received <0.06 m of snow depth accumulation between ground-based and airborne surveys
270 (Table S1). ~~We suggest~~ Based on field observations, ~~two~~ blowing snow and wind redistribution (e.g., Pomeroy and Li, 2000)
271 likely caused the primary sources for the larger lidar snow depth error at ACP poor spatial pattern agreement between excavated
272 depth and lidar depth profiles: (1) blowing snow and wind redistribution (e.g., Pomeroy and Li, 2000), which was observed on
273 a daily basis, and (2) ground subsidence that occurred between the snow on and snow off lidar survey, which was collected
274 on 31 August 2022, near the end of the summer thaw cycle. Seasonal Thaw, which has been observed to drive subsidence up
275 to 0.05 m in this region (Chen et al., 2020), may also contribute, but is challenging to quantify with available observations.

276 Lidar at the boreal forest also exhibited higher uncertainties, yielding an RMSE that was nearly half of the average
277 measured snow depth. However, May et al. (2025) demonstrated that the RMSE could be reduced to 0.12 m at CPCRW by
278 removing anomalous snow depths and areas with anomalous snow depth patterns. Uncertainties tended to be higher for taller
279 vegetation heights (>5 m; Figure 42b), although we note a large range of accuracy for lower vegetation heights (<5 m). This
280 weaker agreement could be due to one or more of four primary factors: (1) snow disturbance due to ground surveys caused
281 errors within the lidar retrieval method, (2) differences in canopy structure between summer and winter acquisitions (e.g., bent-
282 over trees from snow burden), (3) signal penetration through the dense canopy may be problematic for the method (e.g.,
283 Hopkinson et al., 2004), or (4) GNSS location uncertainty between the lidar and excavated depths. Despite the higher
284 uncertainty for the lidar snow depths, the lidar coverage is spatially continuous and complete over the field sites, a clear
285 advantage over the GPR measurements.

286 5.2 Implications for SnowEx23 GPR and Lidar Datasets

287 Although we identified a clear bias for GPR in the boreal forest, it appears that this bias exhibited some dependence upon the
288 land cover, but we were unable to fully evaluate this point. Further work, potentially through a depth probe-GPR evaluation,
289 is needed to identify systematic biases within the boreal forest for GPR operation.

290 ACP lidar snow depths appear to be affected by swath alignment artifacts, which users should be aware of before using
291 the dataset. If the identified bias is removed from the lidar swath by simple subtraction, the ACP lidar RMSE improves from
292 0.20 m to 0.05 m. However, the remaining lidar swaths may be challenging to correct given the lack of independent in situ
293 observations in these swaths. At UKT, lidar snow depths exhibited low bias and relatively high accuracy, whereas lidar snow
294 depths at ~~ACP and~~ the boreal forest sites exhibited a substantial positive bias. Fair et al. (2025⁴) evaluated ICESat-2 lidar snow
295 depths at UKT and FLCF using the airborne lidar snow depths and found better ICESat-2 performance at UKT ($r^2 = 0.84$ –
296 0.92) than at FLCF ($r^2 = 0.14$ – 0.58), further highlighting the boreal forest complexities. In the forests, the lidar snow depth
297 bias is directly related to potential void spaces caused by shrub canopy interception and a lack of photon penetration below
298 canopy and underbrush. In the Arctic tundra, lidar snow depths may be influenced by seasonal thaw cycles. Given the
299 magnitude of snow disturbance associated with in situ surveys, we expect poor agreement between snow pit/excavated
300 measurements and lidar measurements when the field survey preceded the lidar flight (e.g., Figure 33e, n).

301 6 Conclusions

302 Snow is a critical component of the hydrology and ecology of high-latitude terrestrial environments, but distributed snow
303 depths are difficult to measure at high spatial resolution. As part of the NASA SnowEx March 2023 campaign, spatially
304 distributed L-band center-frequency GPR and airborne lidar data were collected and we evaluated snow depth retrievals at the
305 boreal forest and Arctic tundra sites. Biases were observed for both methods and in both environments, but ground-based GPR
306 surveys yielded accurate snow depths, but with lower variability along the profile which was likely caused by the much larger

307 ~~footprint of the radar signal. snow depths yielded higher overall accuracy.~~ GPR, particularly when operated at or near the
308 snowpack surface, is less sensitive to vegetation and snowpack void spaces than the airborne lidar DEM differencing method.
309 ~~The timing of the lidar flights relative to ground surveys complicated our evaluation, but we noted lower accuracy in the boreal~~
310 ~~forest that may have been caused by vegetation preventing the lidar pulse from reaching the bare earth. Although lidar yielded~~
311 ~~accurate snow depths at the UKT site, we identified vertical alignment issues that contributed to~~ ~~We suggest additional~~
312 ~~complications related to the dynamic ground surface may arise for lidar, as exhibited by the~~ a large positive bias at ACP (bias
313 = +0.19 m). The complex surface conditions of the boreal forest and tundra regions challenge established snow observing
314 methods, warranting careful consideration when using these to evaluate novel remote sensing approaches.
315

316 **Author contributions**

317 Conceptualization: D.M., H.P.M., C.V., K.H.G., R.B., T.M., R.W. Data Curation: K.H.G., C.L., R.W., T.M., M.M., R.B.,
318 D.M., B.B. Analysis: K.H.G., R.B., T.M., R.W. Funding Acquisition: D.M., C.V., H.P.M., R.W., R.B., B.B., T.M., K.H.G.
319 Investigation: all authors. Methodology: K.H.G., D.M., T.M., R.W., R.B. Visualization: K.H.G., R.B. Writing – Original Draft
320 Preparation: K.H.G., R.B., D.M. Writing – Review & Editing: all authors.

321 **Acknowledgements**

322 K.H.G was supported by the Colorado State University Honors program. R.B. was supported by NASA FINESST award
323 80NSSC20K1624 and the U.S. Geological Survey Mendenhall Postdoctoral Fellowship Program. D.M., H.P.M., and R.W.
324 were supported by NASA THP award 80NSSC22K1113. We thank Dr. E. Baker, H. Flynn, and N. Latysh for providing
325 insightful comments which improved the clarity of this paper. Any use of trade, firm, or product names is for descriptive
326 purposes only and does not imply endorsement by the U.S. Government.

327 **Data Availability**

328 ~~Boreal Forest~~ GPR transects (Bonnell ~~and McGrath~~ et al., 2025~~4~~; <https://doi.org/10.5067/3X5Q3X7Y87U3>), Arctic Tundra
329 ~~dual polarization GPR transects~~ (Meehan and Rowland, 2024; <https://doi.org/10.5067/TSU0U7L4X2UW>) and single
330 ~~polarization~~ (Webb, 2024; <https://doi.org/10.5067/H3D9IT1W6JT6>), lidar data (Larsen, 2024;
331 <https://doi.org/10.5067/BV4D8RRU1H7U>), and snow pits (Mason et al., 2024; <https://doi.org/413819/SJZ90KNPKCYR>) are
332 archived with the NSIDC DAAC. ~~Creamer's Field SNOTEL data are available at~~

333 <https://wcc.sc.egov.usda.gov/nwcc/site?sitenum=1302>. NOAA AK Deadhorse 3 S weather station data are available at
334 <https://www.ncei.noaa.gov/access/crn/sensors.htm?stationId=1793>.

335

336 **Competing Interests**

337 At least one of the (co-) authors is a member of the editorial board of *The Cryosphere*. The authors have no other competing
338 interests to declare

339 **References**

340 [Aitchison, C. W.: Winter energy requirements of soricine shrews, *Mammal Review*, 17, 25-38, \[https://doi.org/10.1111/j.1365-\]\(https://doi.org/10.1111/j.1365-2907.1987.tb00046.x\)
341 \[2907.1987.tb00046.x\]\(#\), 1987](#)

342 [Benson, C. S.: Polar regions snow cover, *Physics of Snow and Ice: Proceedings*, 1, 1039-1063, 1967.](#)

343 [Benson, C. S. and Sturm, M.: Structure and wind transport of seasonal snow on the Arctic slope of Alaska, *Annals of*
344 \[Glaciology\]\(#\), 18, <https://doi.org/10.3189/S0260305500011629>, 1993.](#)

345 Berezovskaya, S. and Kane, D. L.: Measuring snow water equivalent for hydrological applications: part 1, accuracy
346 observations, 16th International Northern Research Basins Symposium and Workshop, Petrozavodsk, 29-2007.

347 [Bonnell, R., McGrath, D., Detre, A., and Holland-Goon, K.: SnowEx23 Mar23 IOP CSU 1 GHz Ground Penetrating Radar](#)
348 [Raw, Version 1 \[data set\], NASA National Snow and Ice Data Center Distributed Active Archive Center,](#)
349 <https://doi.org/10.5067/3X5Q3X7Y87U3>, 2025.

350 ~~[Bonnell, R. and McGrath, D.: SnowEx23 Colorado State University Ground Penetrating Radar Raw, Version 1 \[data set\],](#)~~
351 ~~[NASA National Snow and Ice Data Center Distributed Active Archive Center, <https://doi.org/10.5067/VGIDSZVEXMSQ>,](#)~~
352 ~~[2024.](#)~~

353 Chen, J. Wu, Y., O'Connor, M., Cardenas, M. B., Schaefer, K., Michaelides, R., and Kling, G.: Active layer freeze-thaw and
354 water storage dynamics in permafrost environments inferred from InSAR, *Remote Sensing of Environment*, 248, 112007,
355 <https://doi.org/10.1016/j.rse.2020.112007>, 2020.

356 Daniels, D. J. (Ed): *Ground Penetrating Radar, Volume 1*, The Institution of Electrical Engineers, 2004.

357 [Duquette, L. S.: Snow Characteristics along Caribou Trails and within Feeding Areas during Spring Migration. *Arctic*, 41,](https://journalhosting.ucalgary.ca/index.php/arctic/article/view/64760/48674)
358 [143-144. https://journalhosting.ucalgary.ca/index.php/arctic/article/view/64760/48674, 1988.](https://journalhosting.ucalgary.ca/index.php/arctic/article/view/64760/48674)

359 Eppler, J., Rabus, B., and Morse, P.: Snow water equivalent change mapping from slope-correlated synthetic aperture radar
360 interferometry (InSAR) phase variations, *The Cryosphere*, 16, 1497–1521, <https://doi.org/10.5194/tc-16-1497-2022>, 2022.

361 Fair, Z., Vuyovich, C., Neumann, T. A., Larsen, C. F., Stuefer, S. L., Mason, M., and May, L: Characterizing ICESat-2 Snow
362 Depths Over the Boreal Forests and Tundra of Alaska in Support of the SnowEx 2023 Campaign ~~[preprint]~~, ~~ESS Open~~
363 ~~Archive~~ [Water Resources Research](https://essopenarchive.org/users/524768/articles/1233703-characterizing-icesat-2-snow-depths-over-the-boreal-forests-and-tundra-of-alaska-in-support-of-the-snowex-2023-campaign), 61, [e2024WR039076](https://doi.org/10.1029/2024WR039076), [https://essopenarchive.org/users/524768/articles/1233703-](https://essopenarchive.org/users/524768/articles/1233703-characterizing-icesat-2-snow-depths-over-the-boreal-forests-and-tundra-of-alaska-in-support-of-the-snowex-2023-campaign)
364 [characterizing-icesat-2-snow-depths-over-the-boreal-forests-and-tundra-of-alaska-in-support-of-the-snowex-2023-campaign,](https://essopenarchive.org/users/524768/articles/1233703-characterizing-icesat-2-snow-depths-over-the-boreal-forests-and-tundra-of-alaska-in-support-of-the-snowex-2023-campaign)
365 [2025](https://essopenarchive.org/users/524768/articles/1233703-characterizing-icesat-2-snow-depths-over-the-boreal-forests-and-tundra-of-alaska-in-support-of-the-snowex-2023-campaign).

366 Jorgensen, T., Yoshikawam K., Kanevskiy, M., Shur, Y., Romanovsky, V., Marchenko, S., Grosse, G., Brown, J., and Jones,
367 B.: Permafrost Characteristics of Alaska [map]
368 https://permafrost.gi.alaska.edu/sites/default/files/AlaskaPermafrostMap_Front_Dec2008_Jorgenson_etal_2008.pdf, 2008.

369 Kelsey, K. C., Pedersen, S. H., Leffler, A. J., Sexton, J. O., Feng, M., and Welker, J. M.: Winter snow and spring temperature
370 have differential effects on vegetation phenology and productivity across Arctic plant communities, *Global Change Biology*,
371 27, 1572–1586, <https://doi.org/10.1111/gcb.15505>, 2021.

372 [Kovacs, A., Gow, A. J., and Morey, R. M.: The in-situ dielectric constant of polar firn revisited. *Cold Regions Science and*
373 *Technology*, 23, 245–256, \[https://doi.org/10.1016/0165-232X\\(94\\)00016-Q\]\(https://doi.org/10.1016/0165-232X\(94\)00016-Q\), 1995.](https://doi.org/10.1016/0165-232X(94)00016-Q)

374 Larsen, C.: SnowEx23 Airborne Lidar-Derived 0.25M Snow Depth and Canopy Height, Version 1 [data set], NASA National
375 Snow and Ice Data Center Distributed Active Archive Center, <https://doi.org/10.5067/BV4D8RRU1H7U>, 2024.

376 Mason, M., Vuyovich, C. M., Stuefer, S., Elder, K., Vas, D., Marshall, H., and Durand, M.: SnowEx23 Mar23 Snow Pit
377 Measurements, Version 1 [data set], NASA National Snow and Ice Data Center Distributed Active Archive Center,
378 <https://doi.org/10.5067/SJZ90KNPKCYR>, 2024

379 [May, L. D., Stuefer, S. L., Goddard, S. D., and Larsen, C. F.: Analyzing vegetation effects on snow depth variability in Alaska’s](https://doi.org/10.5194/tc-19-3477-2025)
380 [boreal forests with airborne lidar, *The Cryosphere*, 19, 3477-3492, https://doi.org/10.5194/tc-19-3477-2025, 2025.](https://doi.org/10.5194/tc-19-3477-2025)

381 [McGrath, D., Webb, R., Shean, D., Bonnell, R., Marshall, H.-P., Painter, T. H., Molotch, N. P., Elder, K., Hiemstra, C., and](https://doi.org/10.1029/2024WR039076)
382 [Brucker, L.: Spatially Extensive Ground-Penetrating Radar Snow Depth Observations During NASA’s 2017 SnowEx](https://doi.org/10.1029/2024WR039076)

383 [Campaign: Comparison With In Situ, Airborne, and Satellite Observations, *Water Resources Research*, 55, 10026–10036,](#)
384 <https://doi.org/10.1029/2019WR024907>, 2019.

385 Meehan, T. G. and Rowland, T.: SnowEx23 CRREL Ground Penetrating Radar, Version 1 [data set], NASA National Snow
386 and Ice Data Center Distributed Active Archive Center, <https://doi.org/10.5067/TSU0U7L4X2UW>, 2024.

387 [Meehan, T. G., Hojatimalekshah, A., Marshall, H.-P., Deeb, E. J., O’Neel, S., McGrath, D., Webb, R. W., Bonnell, R., Raleigh,](#)
388 [M. S., Hiemstra, C., and Elder, K.: Spatially distributed snow depth, bulk density, and snow water equivalent from ground-](#)
389 [based and airborne sensor integration at Grand Mesa, Colorado, USA, *The Cryosphere*, 18, 3253–3276,](#)
390 <https://doi.org/10.5194/tc-18-3253-2024>, 2024.

391 Meredith, M., Sommerkorn, M., Cassotta, S., Derksen, C., Ekaykin, A., Hollowed, A., Kofinas, G., Mackintosh, A.,
392 Melbourne-Thomas, J., Muelbert, M. M. C., Ottersen, G., Pritchard, H., and Schuur, E. A. G.: Polar Regions. IPCC Special
393 Report on the Ocean and Cryosphere in a Changing Climate, 203-320, <https://doi.org/10.1017/9781009157964.005>, 2019.

394 NASA Earth Observatory: Forest on the Threshold, [blog post].
395 https://earthobservatory.nasa.gov/features/BorealThreshold/boreal_threshold4.php, 2006.

396 Obu, J., Westermann, S., Bartsch, A., Berdnikov, N., Christiansen, H. H., Dashtseren, A., Delaloye, R., Elberling, B.,
397 Etzelmüller, B., Kholodov, A., Khomutov, A., Kääb, A., Leibman, M. O., Lewkowitz, A. G., Panda, S. K., Romanovsky, V.,
398 Way, R. G., Westergaard-Nielsen, A., Wu, T., Yamkhin, J., and Zou, D.: Northern Hemisphere permafrost map based on
399 TTOP modelling for 2000–2016 at 1 km² scale, *Earth-Science Reviews*, 193, 233-316,
400 <https://doi.org/10.1016/j.earscirev.2019.04.023>, 2019.

401 Pedersen, S. H., Bentzen, T. W., Reinking, A. K., Liston, G. E., Elder, K., Lenart, E. A., Prichard, A. K., and Welker, J. M.:
402 Quantifying effects of snow depth on caribou winter range selection and movement in Arctic Alaska, *Movement Ecology*, 9,
403 48, <https://doi.org/10.1186/s40462-021-00276-4>, 2021.

404 Penczykowski, R. M., Connolly, B. M., and Barton, B. T.: Winter is changing: Trophic interactions under altered snow
405 regimes, *Food Webs*, 13, 80–91, <https://doi.org/10.1016/j.fooweb.2017.02.006>, 2017.

406 Pomeroy, J. W. and Li, L.: Prairie and arctic areal snow cover mass balance using a blowing snow model, *Journal of*
407 *Geophysical Research: Atmospheres*, 105, 26619-26634, <https://doi.org/10.1029/2000JD900149>, 2000.

408 [Pruitt, W. O., Jr. \(1970\) Some ecological aspects of snow, *Ecology of the Subarctic Regions: Proceedings of the Helsinki*](#)
409 [Symposium, UNESCO, 83-99, <https://unesdoc.unesco.org/ark:/48223/pf0000004082>, 1970.](#)

410 [Stuefer, S. L., Hale, K., May, L. D., Mason, M., Vuyovich, C., Marshall, H. P., Vas, D., and Elder, K.: Snow depth](https://doi.org/10.1038/s41597-025-05430-w)
411 [measurements from Arctic tundra and boreal forest collected during NASA SnowEx Alaska Campaign, Scientific Data, 12,](https://doi.org/10.1038/s41597-025-05430-w)
412 [919, https://doi.org/10.1038/s41597-025-05430-w, 2025.](https://doi.org/10.1038/s41597-025-05430-w)

413 Sturm, M. and Liston, G. E.: Revisiting the Global Seasonal Snow Classification: An Updated Dataset for Earth System
414 Applications, <https://doi.org/10.1175/JHM-D-21-0070.1>, 2021.

415 Vuyovich, C., Stuefer, S., Gleason, K., Durand, M., Marshall, H. P., Osmanoglu, B., Elder, K., Vas, D., Mason, M., Nolin, A.,
416 Youcha, E., Gelvin, A., Larsen, C., Pedersen, S., Hodkinson, D., Deeb, E., and Boyd, D.: NASA SnowEx 2023 Experiment
417 Plan [science plan], [https://snow.nasa.gov/sites/default/files/users/user354/SNEX-](https://snow.nasa.gov/sites/default/files/users/user354/SNEX-Campaigns/2023/NASA_SnowEx_Experiment_Plan_2023_draft_20June2024.pdf)
418 [Campaigns/2023/NASA_SnowEx_Experiment_Plan_2023_draft_20June2024.pdf](https://snow.nasa.gov/sites/default/files/users/user354/SNEX-Campaigns/2023/NASA_SnowEx_Experiment_Plan_2023_draft_20June2024.pdf), 2024.

419 Webb, R.: SnowEx23 University of Wyoming Ground Penetrating Radar, Version 1 [data set]. NASA National Snow and Ice
420 Data Center Distributed Active Archive Center, <https://doi.org/10.5067/H3D9IT1W6JT6>, 2024.

421

422